ACS central science

http://pubs.acs.org/journal/acscii

Research Article

Constructing Well-Defined and Robust Th-MOF-Supported Single-Site Copper for Production and Storage of Ammonia from Electroreduction of Nitrate

Zhi Gao, Yulian Lai, Yuan Tao, Longhui Xiao, Liuxin Zhang, and Feng Luo*

Cite This: *ACS Cent. Sci.* 2021, 7, 1066−1072

Read Online

ACCESS | Metrics & More | Article Recommendations | Supporting Information

ABSTRACT: A combined technique of production and storage of ammonia (NH_3) from electroreduction of nitrate (NO_3^-) through one material is highly desirable but remains a huge challenge. Herein, we proposed a proof-of-concept strategy for combined NH_3 production and storage from electroreduction of NO_3^- through elaborately designing a single-site Cu^{II}-bipyridine-based thorium metal−organic framework (Cu@Th-BPYDC). Noticeably, the single Cu^{II} site, anchored by a solid−liquid postsynthetic metalation within Th-BPYDC, shows a novel square coordination structure, as determined by the single-crystal X-ray diffraction. This strongly implies its enormous potential as an open metal site and consequently enables excellent performance in electroreduction of NO_3^- for NH_3 production, giving 92.5% Faradaic efficiency and 225.3 μmol h^{-1} cm^{-2} yield. Impressively, we can further use Cu@Th-BPYDC material to effectively capture the previously produced NH_3 from electroreduction of NO_3^-, affording an uptake up to 20.55 mmol g^{-1} at 298 K at 1 bar. The results in this work will outline a new direction toward the combined technique for advanced electrocatalysis such as gas production *plus* storage/or separation.

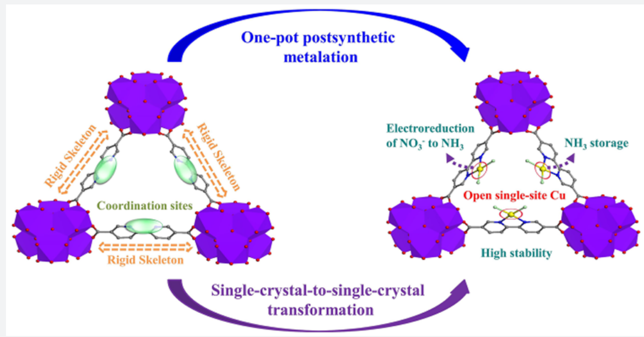

Ammonia (NH_3) is essential for nitrogen fertilizer production and is also regarded as a future green energy carrier because of its high energy density and zero emissions of carbon dioxide.[1,2] Aqueous-based electroreduction of nitrate anion (NO_3^-) to produce NH_3 is a promising technology instead of the traditional energy-intensive Haber−Bosch method owing to the benign conditions. Moreover, the dissociation energy of the N═O bond (204 kJ mol^{-1}) in NO_3^- is lower with respect to the N≡N bond (941 kJ mol^{-1}) in N_2, which enables faster reaction kinetics.[3−5] On the other hand, NO_3^- is abundant in natural environments, especially in effluents, which is harmful to human health and needs to be treated.[6−9] Thus, using NO_3^- as raw material to produce NH_3 by aqueous electroreduction has the potential to simultaneously address energy and environmental issues.

RESULTS AND DISCUSSION

With further use of NH_3, some convenient ways to store it must be developed. In industry, high pressure is often used to compress gas NH_3 to liquid NH_3 in storage tanks for maximized storage density and convenient transportation. However, this is a high energy consumption manner. Thus, in recent years, different porous materials have been developed to store NH_3 due to its low energy consumption and convenient-to-operate manner.[10−13] In general, the adsorbent first must possess high stability owing to the strong corrosivity of NH_3.[14] Second, the special functional groups, especially acidic sites, are generally necessary to strongly interact with basic NH_3 and achieve high total uptake and strong affinity.[15−17] However, at present, NH_3 production and storage were performed separately using different materials. From the perspective of green and sustainable development and the need of future advanced materials, developing a combined technique for production and storage of NH_3 from electroreduction of NO_3^- through one material is highly desirable but remains a huge challenge.

Thanks to the recent reports for electrocatalytic reduction of NO_3^-,[1,2,6,8,18−22] we found that Cu-based materials were more suitable electrocatalysts instead of other metal-based catalysts owing to their efficient inhibiting ability for competitive hydrogen evolution reaction (HER).[23] However, the efficiency of NO_3^- electroreduction to NH_3 still needs to be further improved. Recently, single-site solid catalysts have obtained a

Received: March 24, 2021
Published: June 2, 2021

Scheme 1. Single-Crystal-to-Single-Crystal Transformation and the Advantages of Th-BPYDC (a) and Cu@Th-BPYDC (b)

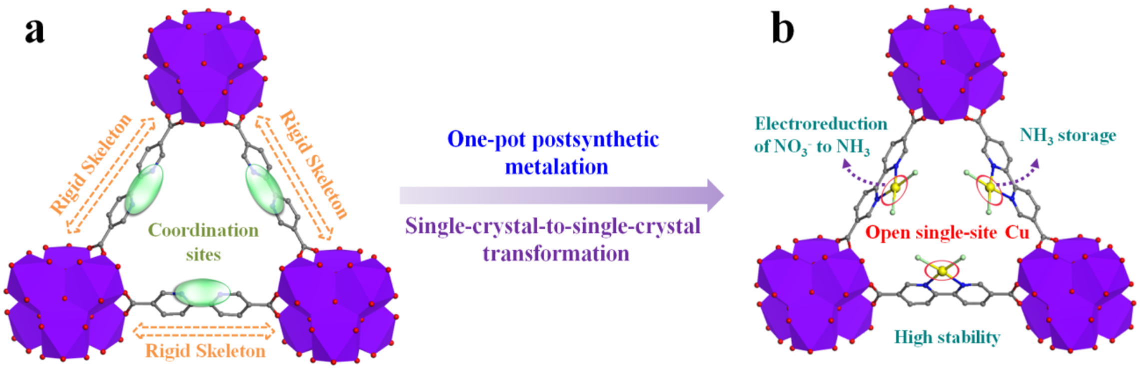

great deal of attention owing to the maximum atom utilization.[24−26] More importantly, the unsaturated coordination environments of single-metal sites have been proved to significantly enhance catalytic activity of different reactions.[27−29] Metal−organic frameworks (MOFs), as emerging coordination polymers with well-defined structure, uniform channel structures, and high surface area, are promising supports to fabricate single-site catalysts.[30−33] The single-metal sites can be deliberately anchored on well-defined positions of MOFs by postsynthetic modification, making them have uniform distribution throughout the MOFs' support. Also, the high density of single-metal sites can be obtained through choosing suitable ligands for active metal anchoring, which is hard to achieve on traditional supports. Thereby, it is reasonable to deduce that deliberately designing MOF-supported open single-site Cu-based solid catalysts can effectively enhance NO_3^- reduction performance but have not been explored.

On the other hand, the open single-site Cu can serve as a Lewis acid site to strongly interact with NH_3 molecules, thus enabling the high NH_3 uptake capacity. However, in the case of NH_3 storage, because of the high toxicity and corrosivity of NH_3, MOFs seem to be inappropriate owing to the poor stability in many MOFs. Excitingly, as recently reported by our group,[34] high-valence Th-based MOFs possess the advantages of ultrahigh stability similar to Zr-based MOFs.[35] More importantly, Th-based MOFs tend to have higher crystallization and a well-defined structure compared to Zr-based MOFs because of their inferior hydrolytic nature,[36] which is good for the theoretical prediction and clarification of relevant mechanisms, allowing for the deliberate regulation and optimization of Th-based MOF single-site materials to achieve a combined technique of production and storage of NH_3 from electroreduction of NO_3^- through one material.

Herein, a solid−liquid postsynthetic modification of crystalline Th-BPYDC was performed to synthesize the robust Th-MOF-supported single-site Cu material (Cu@Th-BPYDC) for NO_3^- electroreduction to produce and store NH_3. Excitingly, the Cu site presents a novel square coordination structure determined by single-crystal X-ray diffraction, indicative of unsaturated coordination. As expected, the Cu@Th-BPYDC presents an excellent performance for NO_3^- electroreduction to produce NH_3 with high yield (225.3 μmol h^{-1} cm^{-2}) and Faradaic efficiency (94.5%). ^{15}N isotope labeling experiments prove that NH_3 originates from NO_3^- reduction. Furthermore, as demonstrated by DFT theoretical calculations and NH_3-TPD, the open single-site Cu serving as a Lewis acid site strongly interacts with NH_3, thus leading to the high uptake capacity of 20.55 mmol g^{-1} at 1 bar at 298 K and 0.335 g/g from the electrolyte after the stability test.

Initially, a Th-MOF single crystal (Th-BPYDC) was synthesized by the solvothermal reaction of $Th(NO_3)_4$ and 2,2′-bipyridine-5,5′-dicarboxylic acid (BPYDC) in the presence of nitric acid and DMF. Then, as shown in Scheme 1, postsynthetic metalation was performed via a second solvothermal reaction between Th-BPYDC and $CuCl_2$ to obtain the Th-MOF-supported single-site Cu material (Cu@Th-BPYDC) crystal.[37] Th-BPYDC exhibits a rigid skeleton and chelating coordination sites, making postsynthetic modification easy to perform (Scheme 1a). The resulting Cu@Th-BPYDC possesses the open single-site Cu, which not only serves as an active site to promote electroreduction NO_3^- to NH_3 but also provides Lewis acid sites to adsorb NH_3 (Scheme 1b). X-ray single-crystal analysis of Th-BPYDC demonstrates that the framework is isostructural to UiO-67 with the cubic space group *Fm3m* (Figure 1a). Noticeably, the single-crystal-to-single-crystal transformation is achieved from Th-BPYDC to Cu@Th-BPYDC, which is hard to achieve generally because the crystallinity of support usually decreases obviously after metalation.[38] As shown in Figure 1b, Cu@Th-BPYDC is also isostructural to UiO-67, indicating no change in the space group upon metalation. Noticeably, the single-site Cu presents planar four-coordination geometry coordinated with two nitrogen atoms of bipyridine in BPYDC *plus* two chlorine atoms, confirming the formation of the open single-site Cu. Moreover, the single-site Cu is uniformly distributed on the Th-BPYDC support.

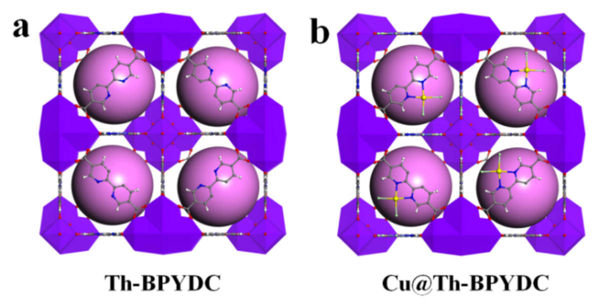

Figure 1. Crystal structures of Th-BPYDC (a) and Cu@Th-BPYDC (b).

XRD measurements were carried out to disclose the purity of Th-BPYDC and Cu@Th-BPYDC. As shown in Figure 2a, the diffraction patterns of them are very similar and match well with the simulated patterns, proving their high purity and

https://doi.org/10.1021/acscentsci.1c00370
ACS Cent. Sci. 2021, 7, 1066−1072

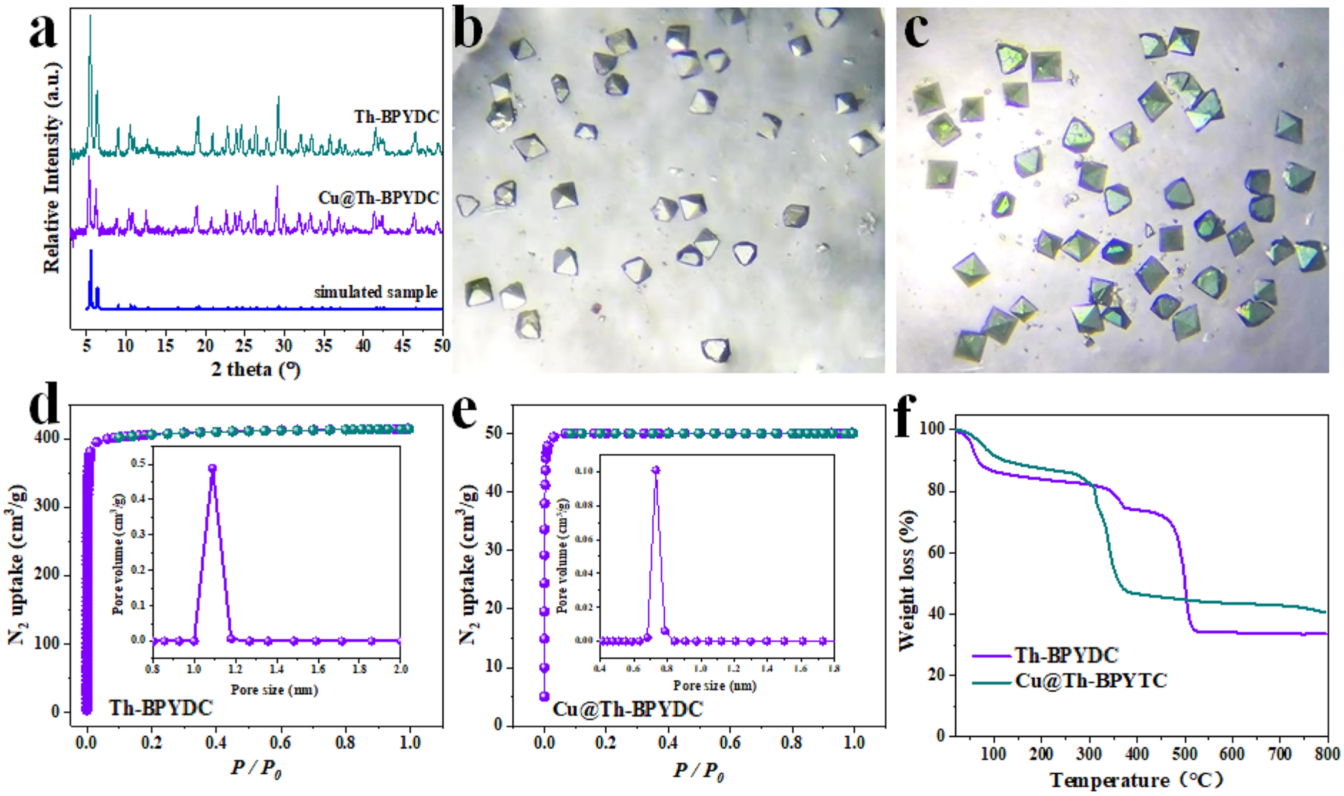

Figure 2. XRD patterns of Th-BPYDC and Cu@Th-BPYDC (a), the optical microscope images of Th-BPYDC (b) and Cu@Th-BPYDC (c), the N_2 adsorption at 77 K with the inset for the distribution of pore size in Th-BPYDC (d) and Cu@Th-BPYDC (e), and thermogravimetric analysis (TGA) curves (f).

crystallinity.[39] The obvious color change before and after metalation was observed by optical microscope images (Figure 2b,c). After metalating with Cu^{2+}, the colorless octahedral crystal in Th-BPYDC is transformed to green, further indicative of the successful incorporation of Cu^{2+} within the framework of Th-BPYDC. The SEM image of Cu@Th-BPYDC further reveals the octahedral morphology (Figure S1), well consistent with the morphology revealed by the optical microscope image (Figure 2c). Low-temperature N_2 adsorption−desorption measurements were performed at 77 K to know the Brunauer−Emmett−Teller (BET) surface areas and pore size distribution. As shown in Figure 2d, the BET surface area of Th-BPYDC is estimated to be 1140 m^2/g, which significantly decreases to 119 m^2/g in Cu@Th-BPYDC (Figure 2e). Density functional theory (DFT) pore size distribution of Th-BPYDC appears at about 1 nm, while in Cu@Th-BPYDC, it decreases to 0.7 nm (inset in Figure 2d,e). The significant change of the BET surface area and pore size distribution further reveals the incorporation of Cu^{2+}. Thermogravimetric analysis (TGA) curves of Th-BPYDC and Cu@Th-BPYDC tested under the air flow were compared (Figure 2f). They remain stable even up to about 300 °C, exhibiting high thermal stability. The weight loss in Th-BPYDC is 66.4 wt %, which decreases to 59.5 wt % owing to the incorporation of Cu species. The Cu loading is calculated to be about 7.1 wt %, well consistent with the result determined by ICP-AES measurement (7.2 wt %), indicating the high density of the single-site Cu. Furthermore, the N content in Cu@Th-BPYDC is determined by elemental microanalysis to be about 6.32 wt %. The molar ratio of N/Cu is calculated to be about 4.0. Thus, the occupancy of bipyridine sites by Cu is 50%. On the basis of the above characterization results, we conclude that Cu@Th-BPYDC with the open single-site Cu and well-defined crystalline structure was successfully synthesized, in which the Cu sites are very uniform and present high density.

The performance for electrocatalytic nitrate reduction to ammonia was investigated in the 1 M KOH + 100 mM KNO_3 (pH = 14) electrolyte. Colorimetric methods were used to determine the concentration of NH_3. Before measurement, multiple linear sweep voltammetry (LSV) tests were performed to obtain unchanged polarization curves. As shown in Figure 3a, the LSV curves of Cu@Th-BPYDC reflect a rapid increase of current density after adding KNO_3, demonstrating that NO_3^- in electrolytes involves the reduction reaction. The distinct difference for the chromogenic results of the electrolyte with and without KNO_3 tested by Nessler's reagents after the reaction was shown, proving the generation of NH_3 (Figures S2 and S3). Noticeably, the Cu-free Th-BPYDC presents negligible activity toward NO_3^- electroreduction, while at the potential of −0.1 V vs RHE, the density of Cu@Th-BPYDC reaches as high as 80.7 mA cm^{-2}. Further, the LSV curves normalized to the electrochemically active surface area (ECSA) were plotted. As determined by double-layer capacitance (C_{dl}), the ECSA of Th-BPYDC is very similar to that of Cu@Th-BPYDC (Figure S4). As a result, the ECSA-normalized current density at −0.1 V vs RHE in Cu@Th-BPYDC is as high as 88.4-fold higher than that in Th-BPYDC (Figure S5), proving the significant improvement of intrinsic activity after incorporating the single-site Cu.

The electrical conductivity of materials has a significant effect on electrocatalytic activity. Thus, the electrical

https://doi.org/10.1021/acscentsci.1c00370
ACS Cent. Sci. 2021, 7, 1066−1072

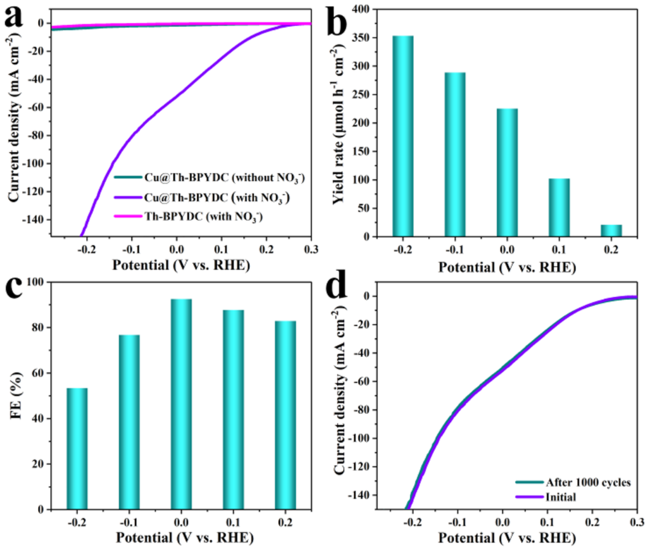

Figure 3. LSV curves (a), NH_3 yield rate (b) and Faradaic efficiency (c) at different potentials, and LSV curves for Cu@Th-BPYDC before and after 1000 cycles of CV scans (d).

conductivity of Th-BPYDC and Cu@Th-BPYDC was first measured to explore the origin of obviously different activity. The results indicate that Th-BPYDC support presents very poor conductivity (1×10^{-9} S cm^{-1}). However, after incorporation of high-density single-site Cu, the conductivity increases significantly to 2.3×10^{-4} S cm^{-1}, about a 5 order of magnitude improvement. This significant enhancement of conductivity is mainly ascribed to the intervalence charge transfer and overlapped band gaps originating from redox-active Cu species.[40−43] Moreover, incorporating single-site Cu on BPYDC also can result in the energetic overlap between Th_6 nodes and the ligand, thus promoting the charge transport by the "through-bond" route.[44] The electrochemical impedance spectroscopy (EIS) measurements were also carried out. As revealed by Nyquist curves in Figure S6, incorporating single-site Cu into Th-BPYDC can significantly decrease the interfacial charge transfer resistance between catalysts and electrolyte,[45] which implies the enhanced conductivity of Cu@Th-BPYDC, well consistent with the results of electrical conductivity in Th-BPYDC and Cu@Th-BPYDC.

The effects of different potentials on the yield rates and Faradaic efficiency of NH_3 were investigated. As shown in Figure 3b, the yield rate of NH_3 production gradually increases with the improvement of cathodic potential. However, the Faradaic efficiency toward NH_3 production shows a volcanic shaped curve. At 0 V vs RHE, the NH_3 Faradaic efficiency reaches a maximum of 92.5% (Figure 3c). Further increasing of the potential results in the decrease of Faradaic efficiency, which should be ascribed to the enhancement of the competitive hydrogen evolution reaction (HER). Thus, 0 V vs RHE is deemed the optimal potential comprehensively considering the yield rate (225.3 μmol h^{-1} cm^{-2}) and Faradaic efficiency (92.5%) of NH_3. To our knowledge, the yield rate and Faradaic efficiency of NH_3 production presented here are superior to the values reported in most electrocatalysts (Table S1).

$^{15}NO_3^-$ isotope labeling experiments were carried out to determine that NH_3 originates from NO_3^- rather than from other potential sources such as atmosphere and electrolyte. The electrolyte after a reaction of 1 h was collected, followed by ^{1}H NMR measurement. The spectra using $^{15}NO_3^-$ as the electrolyte only present two peaks at $\delta = 6.97$ and 7.09 ppm, which undoubtedly confirms that the as-synthesized NH_3 originates from NO_3^- electroreduction (Figure S7).[18−20] The stability of electrocatalysts is a crucial criterion to assess the practical application prospect. As presented in Figure 3d, no significant decrease of electrocatalytic activity was observed after 1000 CV cycles, further determining the outstanding stability of Cu@Th-BPYDC for NO_3^- electroreduction. The XRD measurement of Cu@Th-BPYDC after the stability test was carried out, which remains nearly identical to that before (Figure S8). Moreover, the ICP-AES result indicates the unchanged Cu content of Cu@Th-BPYDC before and after the stability test of NO_3^- electroreduction. The BET surface area measurement of Cu@Th-BPYDC after NO_3^- electroreduction was performed. As shown in Figure S9, the BET surface area of Cu@Th-BPYDC after the stability test for NO_3^- electroreduction is 110 m^2/g, which is almost identical to that of fresh Cu@Th-BPYDC (119 m^2/g).

Meanwhile, NH_3 uptake capacities of Cu@Th-BPYDC and Cu-free Th-BPYDC were tested in a broad range of NH_3 concentrations at 298 K. As determined by NH_3 isotherms (Figure 4a), with the increase in the NH_3 pressure, NH_3 uptake quickly increases in the low-pressure region and then gradually increases to the maximal value in Cu@Th-BPYDC. In the case of Cu-free Th-BPYDC, NH_3 uptake increases slowly with NH_3 pressure. At 1 bar of NH_3 pressure, the uptake capacities of Cu@Th-BPYDC reach as high as 20.55 mmol g^{-1}, which is as high as 3.5 times higher than that in Th-BPYDC (5.90 mmol g^{-1}). This high uptake capacity is superior to those in most of the recently reported top-performing MOFs and porous polymers (Table S2).[14,17,46−50] The significantly different NH_3 uptake capacities in Cu@Th-BPYDC and Cu-free Th-BPYDC strongly demonstrate that the open single-metal site Cu which serves as a Lewis acid site strongly interacts with NH_3 molecules to improve the NH_3 uptake capacity despite smaller BET surface areas in Cu@Th-

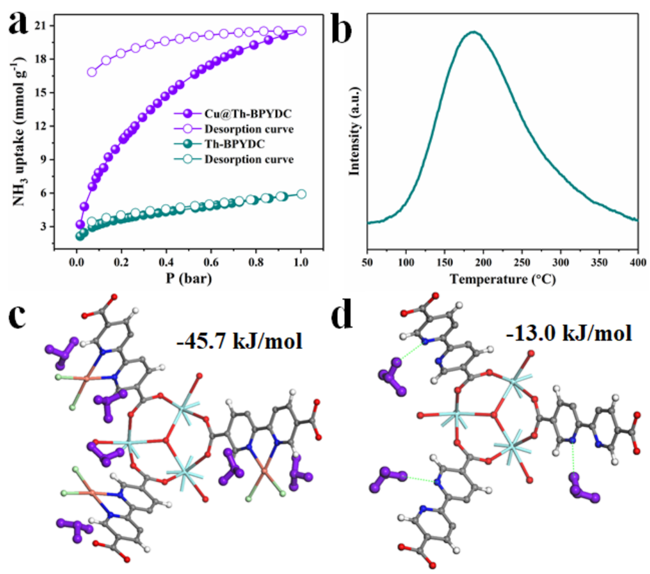

Figure 4. NH_3 adsorption isotherms of Cu@Th-BPYDC and Th-BPYDC (a), NH_3-TPD of Cu@Th-BPYDC (b), and the adsorption of NH_3 on Cu sites in Cu@Th-BPYDC (c) and bipyridine N in Th-BPYDC (d).

https://doi.org/10.1021/acscentsci.1c00370
ACS Cent. Sci. 2021, 7, 1066−1072

BPYDC. Noticeably, the desorption isotherm of Cu@Th-BPYDC does not coincide with the adsorption curve (Figure 4a), indicating an irreversible interaction between Cu sites and NH_3 molecules without any treatment and the formation of chemisorption. Furthermore, Cu@Th-BPYDC after the NH_3 uptake measurement was regenerated after heating at 100 °C for 6 h, and the reusability toward NH_3 uptake was tested. As shown in Figure S10, the NH_3 uptake capacity of Cu@Th-BPYDC is almost unchanged after three consecutive runs. Also, the crystalline structure of Cu@Th-BPYDC after NH_3 uptake is well maintained without detectable collapse, which further proves the excellent stability of Cu@Th-BPYDC (Figure S11). Cu@Th-BPYDC after NH_3 uptake was treated at 100 °C for 6 h, followed by measuring the BET surface area (Figure S12). The result reveals the almost unchanged surface area (105 m^2/g). To further assess the open Cu sites which serve as Lewis acids to promote the affinity of NH_3, NH_3-TPD measurements were carried out.[51] As shown in Figure 4b, a broad single peak was obtained in Cu@Th-BPYDC with the surface acid sites of 0.108 mmol/g originating from open Cu sites. The asymmetric curves indicate that the desorption kinetics follows a first-order reaction, in which the desorption process proceeds on surface exposed acid sites but does not react and combine on the surface.[52−55] Moreover, DFT theoretical calculations were carried out to further disclose the intrinsic reason for significantly different NH_3 uptake capacities in Cu@Th-BPYDC and Th-BPYDC. As shown in Figure 4c,d, the calculated binding energy of NH_3 absorbed on isolated open Cu metal sites in Cu@Th-BPYDC (−45.7 kJ/mol) is much higher than that on bipyridine N in Cu-free Th-BPYDC (−13.0 kJ/mol), undoubtedly determining that the high uptake capacity originates from the strong binding ability of the open Cu site to NH_3 molecules.

Moreover, the uptake ability of Cu@Th-BPYDC toward NH_3 and H_2O in electrolytes after the stability test of NO_3^- electroreduction was tested. To accurately determine the NH_3 uptake capacity from electrolytes, the pure H_2O vapor uptake capacity was also tested. After adsorption of 1 h, the NH_3 uptake capacity reaches 0.123 g/g, about 36.7% of the maximum NH_3 uptake capacity (0.335 g/g), confirming the fast kinetics, while the uptake toward H_2O vapor is negligible (Figure 5a) with the inset for the obvious color change from green in fresh Cu@Th-BPYDC to blue after humid NH_3 uptake. To explain the color change and adsorption mechanism, the FT-IR measurement was performed under ambient conditions. As shown in Figure 5b, after humid NH_3 uptake, new peaks assigned to degenerated and symmetric deformations of Cu-NH_3 at 1625 cm^{-1} were detected, which demonstrates that NH_3 is coordinated to the open Cu metal sites.[14]

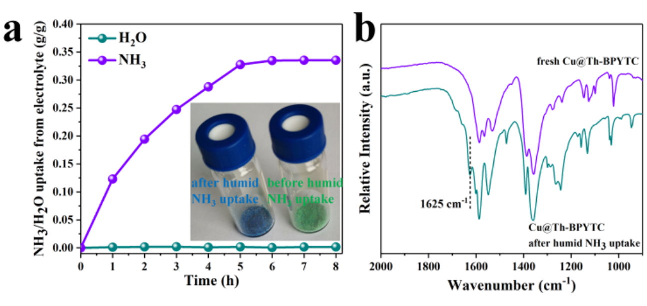

Figure 5. NH_3/H_2O uptake of Cu@Th-BPYDC toward electrolytes after the stability test of NO_3^- electroreduction (a) with the inset for the color of Cu@Th-BPYDC before and after humid NH_3 uptake and FT-IR spectra of Cu@Th-BPYDC before and after humid NH_3 uptake (b).

On the basis of the above experimental and characterization results, the outstanding ability for production and storage of NH_3 from electroreduction of NO_3^- in Cu@Th-BPYDC is mainly ascribed to the following factors. First, the Cu species in Cu@Th-BPYDC presents unsaturated coordination, which is highly active for electrocatalysis. Second, the Cu sites in Cu@Th-BPYDC show high dispersity and density, which provide more accessible active sites for NO_3^- electroreduction. Third, the open single-site Cu can serve as a Lewis acid site to interact with NH_3 molecules and thus enhance NH_3 storage capacity.

■ CONCLUSION

In summary, single-site Cu incorporated within the framework of Th-BPYDC (Cu@Th-BPYDC) was obtained by a simple one-pot postsynthetic metalation. Noticeably, single-crystal-to-single-crystal transformation was achieved from Th-BPYDC to Cu@Th-BPYDC after metalation. The Cu sites in Cu@Th-BPYDC present planar four-coordination configurations and thus are open single-metal sites. The isolated open single-site Cu in Cu@Th-BPYDC can serve as a catalytic active site to promote electrocatalytic NO_3^- reduction to produce NH_3 with high Faradaic efficiency (92.5%) and NH_3 yield (225.3 μmol h^{-1} cm^{-2}). Also, as proved by DFT theoretical calculations and NH_3-TPD, the open single-site Cu species serve as Lewis acid centers to enhance the interaction with NH_3 molecules. Therefore, Cu@Th-BPYDC shows high storage capacity (20.55 mmol g^{-1} at 298 K at 1 bar and 0.335 g/g from electrolyte after the stability test). This work provides a clear path to design MOF materials for a combined technique of NH_3 production and storage by controlling the stability and the property of open single-metal sites.

■ ASSOCIATED CONTENT

Supporting Information

The Supporting Information is available free of charge at https://pubs.acs.org/doi/10.1021/acscentsci.1c00370.

Additional data and figures including SEM image, chromogenic results, linear standard curve, CV plots, ECSA-normalized current densities, Nyquist plots, ^1H NMR spectrum, XRD patterns, N_2 adsorption curves, and reusability toward NH_3 uptake (PDF)

■ AUTHOR INFORMATION

Corresponding Author

Feng Luo − *State Key Laboratory of Nuclear Resources and Environment, School of Biology, Chemistry and Material Science, East China University of Technology, Nanchang, Jiangxi 330013, China;* orcid.org/0000-0001-6380-2754; Email: ecitluofeng@163.com

Authors

Zhi Gao − *State Key Laboratory of Nuclear Resources and Environment, School of Biology, Chemistry and Material Science, East China University of Technology, Nanchang, Jiangxi 330013, China*

Yulian Lai − *State Key Laboratory of Nuclear Resources and Environment, School of Biology, Chemistry and Material*

Science, East China University of Technology, Nanchang, Jiangxi 330013, China
Yuan Tao − *State Key Laboratory of Nuclear Resources and Environment, School of Biology, Chemistry and Material Science, East China University of Technology, Nanchang, Jiangxi 330013, China*
Longhui Xiao − *State Key Laboratory of Nuclear Resources and Environment, School of Biology, Chemistry and Material Science, East China University of Technology, Nanchang, Jiangxi 330013, China*
Liuxin Zhang − *State Key Laboratory of Nuclear Resources and Environment, School of Biology, Chemistry and Material Science, East China University of Technology, Nanchang, Jiangxi 330013, China*

Complete contact information is available at:
https://pubs.acs.org/10.1021/acscentsci.1c00370

Notes

The authors declare no competing financial interest.

■ ACKNOWLEDGMENTS

We thank the Natural Science Foundation of Jiangxi Province of China (20181ACB20003), the Open Fund of State Key Laboratory of Nuclear Resources and Environment (2020NRE30), the Foundation of Jiangxi Educational Committee (GJJ200731), and the Training Program for Academic and Technical Leaders of Major Disciplines in Jiangxi Province (20194BCJ22010).

■ REFERENCES

(1) Chen, G.-F; Yuan, Y.; Jiang, H.; Ren, S.-Y; Ding, L.-X; Ma, L.; Wu, T.; Lu, J.; Wang, H. Electrochemical Reduction of Nitrate to Ammonia via Direct Eight-Electron Transfer Using a Copper−Molecular Solid Catalyst. *Nat. Energy* **2020**, *5*, 605−613.
(2) Wang, Y.; Zhou, W.; Jia, R.; Yu, Y.; Zhang, B. Unveiling the Activity Origin of a Copper-Based Electrocatalyst for Selective Nitrate Reduction to Ammonia. *Angew. Chem., Int. Ed.* **2020**, *59*, 5350−5354.
(3) Seh, Z. W.; Kibsgaard, J.; Dickens, C. F.; Chorkendorff, I.; Norskov, J. K.; Jaramillo, T. F. Combining Theory and Experiment in Electrocatalysis: Insights into Materials Design. *Science* **2017**, *355*, eaad4998.
(4) Rosca, V.; Duca, M.; de Groot, M. T.; Koper, M. T. Nitrogen Cycle Electrocatalysis. *Chem. Rev.* **2009**, *109*, 2209−2244.
(5) Hirakawa, H.; Hashimoto, M.; Shiraishi, Y.; Hirai, T. Selective Nitrate-to-Ammonia Transformation on Surface Defects of Titanium Dioxide Photocatalysts. *ACS Catal.* **2017**, *7*, 3713−3720.
(6) Li, J.; Zhan, G.; Yang, J.; Quan, F.; Mao, C.; Liu, Y.; Wang, B.; Lei, F.; Li, L.; Chan, A. W. M.; Xu, L.; Shi, Y.; Du, Y.; Hao, W.; Wong, P. K.; Wang, J.; Dou, S.-X.; Zhang, L.; Yu, J. C. Efficient Ammonia Electrosynthesis from Nitrate on Strained Ruthenium Nanoclusters. *J. Am. Chem. Soc.* **2020**, *142*, 7036−7046.
(7) Liu, J.-X.; Richards, D.; Singh, N.; Goldsmith, B. R. Activity and Selectivity Trends in Electrocatalytic Nitrate Reduction on Transition Metals. *ACS Catal.* **2019**, *9*, 7052−7064.
(8) Jia, R.; Wang, Y.; Wang, C.; Ling, Y.; Yu, Y.; Zhang, B. Boosting Selective Nitrate Electroreduction to Ammonium by Constructing Oxygen Vacancies in TiO_2. *ACS Catal.* **2020**, *10*, 3533−3540.
(9) Garcia-Segura, S.; Lanzarini-Lopes, M.; Hristovski, K.; Westerhoff, P. Electrocatalytic Reduction of Nitrate: Fundamentals to Full-Scale Water Treatment Applications. *Appl. Catal., B* **2018**, *236*, 546−568.
(10) Jiang, J. C.; Yaghi, O. M. Brønsted Acidity in Metal−Organic Frameworks. *Chem. Rev.* **2015**, *115*, 6966−6997.
(11) Mounfield, W. P.; Claure, M. T.; Agrawal, P. K.; Jones, C. W.; Walton, K. S. Synergistic Effect of Mixed Oxide on the Adsorption of Ammonia with Metal−Organic Frameworks. *Ind. Eng. Chem. Res.* **2016**, *55*, 6492−6500.
(12) Rieth, A. J.; Tulchinsky, Y.; Dinca, M. High and Reversible Ammonia Uptake in Mesoporous Azolate Metal−Organic Frameworks with Open Mn, Co, And Ni Sites. *J. Am. Chem. Soc.* **2016**, *138*, 9401−9404.
(13) Qajar, A.; Peer, M.; Andalibi, M. R.; Rajagopalan, R.; Foley, H. C. Enhanced Ammonia Adsorption on Functionalized Nanoporous Carbons. *Microporous Mesoporous Mater.* **2015**, *218*, 15−23.
(14) Kim, D. W.; Kang, D. W.; Kang, M.; Lee, J.-H.; Choe, J. H.; Chae, Y. S.; Choi, D. S.; Yun, H.; Hong, C. S. High Ammonia Uptake of a Metal−Organic Framework Adsorbent in a Wide Pressure Range. *Angew. Chem.* **2020**, *132*, 22720−22725.
(15) Petit, C.; Bandosz, T. J. Enhanced Adsorption of Ammonia on Metal-Organic Framework/Graphite Oxide Composites: Analysis of Surface Interactions. *Adv. Funct. Mater.* **2010**, *20*, 111.
(16) Van Humbeck, J. F.; McDonald, T. M.; Jing, X.; Wiers, B. M.; Zhu, G.; Long, J. R. Ammonia Capture in Porous Organic Polymers Densely Functionalized with Brønsted Acid Groups. *J. Am. Chem. Soc.* **2014**, *136*, 2432−2440.
(17) Rieth, A. J.; Dincă, M. Controlled Gas Uptake in Metal−Organic Frameworks with Record Ammonia Sorption. *J. Am. Chem. Soc.* **2018**, *140*, 3461−3466.
(18) Yu, Y.; Wang, C.; Yu, Y.; Wang, Y.; Zhang, B. Promoting Selective Electroreduction of Nitrates to Ammonia over Electron-Deficient Co Modulated by Rectifying Schottky Contacts. *Sci. China: Chem.* **2020**, *63*, 1469−1476.
(19) Niu, H.; Zhang, Z.; Wang, X.; Wan, X.; Shao, C.; Guo, Y. Theoretical Insights into the Mechanism of Selective Nitrate-to-Ammonia Electroreduction on Single-Atom Catalysts. *Adv. Funct. Mater.* **2021**, *31*, 2008533.
(20) Ma, X.; Li, M.; Liu, X.; Wang, L.; Chen, N.; Li, J.; Feng, C. A Graphene Oxide Nanosheet-Modified Ti Nanocomposite Electrode with Enhanced Electrochemical Property and Stability for Nitrate Reduction. *Chem. Eng. J.* **2018**, *348*, 171−179.
(21) Wang, Y.; Xu, A.; Wang, Z.; Huang, L.; Li, J.; Li, F.; Wicks, J.; Luo, M.; Nam, D.-H.; Tan, C.-S.; Ding, Y.; Wu, J.; Lum, Y.; Dinh, C.-T.; Sinton, D.; Zheng, G.; Sargent, E. H. J. *J. Am. Chem. Soc.* **2020**, *142*, 5702−5708.
(22) Zhang, X.; Wang, Y.; Liu, C.; Yu, Y.; Lu, S.; Zhang, B. Recent Advances in Non-Noble Metal Electrocatalysts for Nitrate Reduction. *Chem. Eng. J.* **2021**, *403*, 126269.
(23) Wang, Y.; Yu, Y.; Jia, R.; Zhang, C.; Zhang, B. Electrochemical Synthesis of Nitric Acid from Air and Ammonia through Waste Utilization. *Natl. Sci. Rev.* **2019**, *6*, 730−738.
(24) Zhang, H. B.; Liu, G. G.; Shi, L.; Ye, J. H. Single-Atom Catalysts: Emerging Multifunctional Materials in Heterogeneous Catalysis. *Adv. Energy Mater.* **2018**, *8*, 1701343.
(25) Rogge, S. M. J.; Bavykina, A.; Hajek, J.; Garcia, H.; Olivos-Suarez, A. I.; Sepulveda-Escribano, A.; Vimont, A.; Clet, G.; Bazin, P.; Kapteijn, F.; Daturi, M.; Ramos-Fernandez, E. V.; Xamena, F. X. L. i; Speybroeck, V. V.; Gascon, J. Metal−Organic and Covalent Organic Frameworks as Single-Site Catalysts. *Chem. Soc. Rev.* **2017**, *46*, 3134−3184.
(26) Li, B.; Ju, Z.; Zhou, M.; Su, K.; Yuan, D. A Reusable MOF-Supported Single-Site Zinc(II) Catalyst for Efficient Intramolecular Hydroamination of *o*-Alkynylanilines. *Angew. Chem., Int. Ed.* **2019**, *58*, 7687−7691.
(27) Qiao, B.; Wang, A.; Yang, X.; Allard, L. F.; Jiang, Z.; Cui, Y.; Liu, J.; Li, J.; Zhang, T. Single-Atom Catalysis of CO Oxidation Using Pt_1/FeO_x. *Nat. Chem.* **2011**, *3*, 634−641.
(28) Liu, G.; Robertson, A. W.; Li, M. M.; Kuo, W. C. H.; Darby, M. T.; Muhieddine, M. H.; Lin, Y. C.; Suenaga, K.; Stamatakis, M.; Warner, J. H.; Tsang, S. C. E. MoS_2 Monolayer Catalyst Doped with Isolated Co Atoms for the Hydrodeoxygenation Reaction. *Nat. Chem.* **2017**, *9*, 810−816.
(29) Wang, A.; Li, J.; Zhang, T. Heterogeneous Single-Atom Catalysis. *Nat. Rev. Chem.* **2018**, *2*, 65−81.

(30) Song, Y.; Li, Z.; Ji, P.; Kaufmann, M.; Feng, X.; Chen, J. S.; Wang, C.; Lin, W. Metal−Organic Framework Nodes Support Single-Site Nickel(II) Hydride Catalysts for the Hydrogenolysis of Aryl Ethers. *ACS Catal.* **2019**, *9*, 1578−1583.

(31) Gao, Z.; Yu, Z. W.; Liu, F. Q.; Yang, C.; Yuan, Y. H.; Yu, Y.; Luo, F. Stable Iron Hydroxide Nanosheets@Cobalt-Metal−Organic−Framework Heterostructure for Efficient Electrocatalytic Oxygen Evolution. *ChemSusChem* **2019**, *12*, 4623−4628.

(32) Gao, Z.; Xiao, L.; Su, X.; He, X.; Yu, Y.; Huang, X.; Luo, F. Carambola-Like Metal-Organic Frameworks for High-Performance Electrocatalytic Oxygen Evolution Reaction. *J. Energy Chem.* **2021**, *53*, 358−363.

(33) Ji, P.; Manna, K.; Lin, Z.; Feng, X.; Urban, A.; Song, Y.; Lin, W. Single-Site Cobalt Catalysts at New $Zr_{12}(\mu_3\text{-O})_8(\mu_3\text{-OH})_8(\mu_2\text{-OH})_6$ Metal−Organic Framework Nodes for Highly Active Hydrogenation of Nitroarenes, Nitriles, and Isocyanides. *J. Am. Chem. Soc.* **2017**, *139*, 7004−7011.

(34) Xu, Z.; Xiong, X.; Xiong, J.; Krishna, R.; Li, L.; Fan, Y.; Luo, F.; Chen, B. A robust Th-Azole Framework for Highly Efficient Purification of C_2H_4 from a $C_2H_4/C_2H_2/C_2H_6$ Mixture. *Nat. Commun.* **2020**, *11*, 3163.

(35) Xu, H.; Cao, C.-S.; Hu, H.-S.; Wang, S.-B.; Liu, J.-C.; Cheng, P.; Kaltsoyannis, N.; Li, J.; Zhao, B. High Uptake of ReO_4^- and CO_2 Conversion by a Radiatio-Resistant Thorium−Nickle $[Th_{48}Ni_6]$ Nanocage-Based Metal−Organic Framework. *Angew. Chem., Int. Ed.* **2019**, *58*, 6022−6027.

(36) Wang, Y.; Liu, W.; Bai, Z.; Zheng, T.; Silver, M. A.; Li, Y.; Wang, Y.; Wang, X.; Diwu, J.; Chai, Z.; Wang, S. Employing an Unsaturated Th^{4+} Site in a Porous Thorium−Organic Framework for Kr/Xe Uptake and Separation. *Angew. Chem., Int. Ed.* **2018**, *57*, 5783−5787.

(37) Gonzalez, M. I.; Bloch, E. D.; Mason, J. A.; Teat, S. J.; Long, J. R. Single-Crystal-to-Single-Crystal Metalation of a Metal−Organic Framework: A Route toward Structurally Well-Defined Catalysts. *Inorg. Chem.* **2015**, *54*, 2995−3005.

(38) Wang, X.-N.; Zhang, P.; Kirchon, A.; Li, J.-L.; Chen, W.-M.; Zhao, Y.-M.; Li, B.; Zhou, H.-C. Crystallographic Visualization of Postsynthetic Nickel Clusters into Metal−Organic Framework. *J. Am. Chem. Soc.* **2019**, *141*, 13654−13663.

(39) Liu, F. Q.; Liu, J. W.; Gao, Z.; Wang, L.; Fu, X.-Z.; Yang, L. X.; Tao, Y.; Yin, W. H.; Luo, F. Constructing BimetalComplex Based Hydrogen-Bonded Framework for Highly Efficient Electrocatalytic Water Splitting. *Appl. Catal., B* **2019**, *258*, 117973−11800.

(40) Xie, L. S.; Sun, L.; Wan, R.; Park, S. S.; DeGayner, J. A.; Hendon, C. H.; Dincă, M. Tunable Mixed-Valence Doping toward Record Electrical Conductivity in a Three-Dimensional Metal−Organic Framework. *J. Am. Chem. Soc.* **2018**, *140* (24), 7411−7414.

(41) Park, J. G.; Aubrey, M. L.; Oktawiec, J.; Chakarawet, K.; Darago, L. E.; Grandjean, F.; Long, G. J.; Long, J. R. Charge Delocalization and Bulk Electronic Conductivity in the Mixed-Valence Metal−Organic Framework $Fe(1,2,3\text{-triazolate})_2(BF_4)_x$. *J. Am. Chem. Soc.* **2018**, *140* (27), 8526−8534.

(42) Okubo, T.; Anma, H.; Tanaka, N.; Himoto, K.; Seki, S.; Saeki, A.; Maekawa, M.; Kuroda-Sowa, T. Crystal Structure and Carrier Transport Properties of a New Semiconducting 2D Coordination Polymer with a 3,5-Dimethylpiperidine Dithiocarbamate Ligand. *Chem. Commun.* **2013**, *49*, 4316−4318.

(43) Wu, Z.-L.; Wang, C.-H.; Zhao, B.; Dong, J.; Lu, F.; Wang, W.-H.; Wang, W.-C.; Wu, G.-J.; Cui, J.-Z.; Cheng, P. *Angew. Chem., Int. Ed.* **2016**, *55*, 4938−4942.

(44) Meng, H.; Han, Y.; Zhou, C.; Jiang, Q.; Shi, X.; Zhan, C.; Zhang, R. Conductive Metal−Organic Frameworks: Design, Synthesis, and Applications. *Small Methods* **2020**, *4*, 2000396.

(45) Gao, Z.; Yu, Z. W.; Huang, Y.; He, X.; Su, X.; Xiao, L.; Yu, Y.; Huang, X.; Luo, F. Flexible and Robust Bimetallic Covalent Organic Frameworks for the Reversible Switching of Electrocatalytic Oxygen Evolution Activity. *J. Mater. Chem. A* **2020**, *8*, 5907−5912.

(46) Glomb, S.; Woschko, D.; Makhloufi, G.; Janiak, C. Metal−Organic Frameworks with Internal Urea-Functionalized Dicarboxylate Linkers for SO_2 and NH_3 Adsorption. *ACS Appl. Mater. Interfaces* **2017**, *9*, 37419−37434.

(47) Kajiwara, T.; Higuchi, M.; Watanabe, D.; Higashimura, H.; Yamada, T.; Kitagawa, H. A Systematic Study on the Stability of Porous Coordination Polymers against Ammonia. *Chem. - Eur. J.* **2014**, *20*, 15611−15617.

(48) Barin, G.; Peterson, G. W.; Crocella, V.; Xu, J.; Colwell, K. A.; Nandy, A.; Reimer, J. A.; Bordiga, S.; Long, J. R. *Chem. Sci.* **2017**, *8*, 4399−4409.

(49) Doonan, C. J.; Tranchemontagne, D. J.; Glover, T. G.; Hunt, J. R.; Yaghi, O. M. *Nat. Chem.* **2010**, *2*, 235−238.

(50) Yang, Y.; Faheem, M.; Wang, L.; Meng, Q.; Sha, H.; Yang, N.; Yuan, Y.; Zhu, G. *ACS Cent. Sci.* **2018**, *4*, 748−754.

(51) Gao, Z.; Li, C.; Fan, G.; Yang, L.; Li, F. Nitrogen-Doped Carbon-Decorated Copper Catalyst for Highly Efficient Transfer Hydrogenolysis of 5-Hydroxymethylfurfural to Convertibly Produce 2,5-Dimethylfuran or 2,5-Dimethyltetrahydrofuran. *Appl. Catal., B* **2018**, *226*, 523−533.

(52) Holmes Parker, D.; Jones, M. E.; Koel, B. E. Determination of the Reaction Order and Activation Energy for Desorption Kinetics Using TPD Spectra: Application to D_2 Desorption from Ag(111). *Surf. Sci.* **1990**, *233*, 65−73.

(53) Bhattacharyya, K. G. Adsorption of Ammonia on Mica Surfaces. *Langmuir* **1992**, *8*, 2284−2289.

(54) Wu, M. C.; Truong, C. M.; Goodman, D. W. Interactions of Ammonia with a Nickel Oxide (100) Surface Studied by High-Resolution Electron Energy Loss Spectroscopy and Temperature Programmed Desorption Spectroscopy. *J. Phys. Chem.* **1993**, *97*, 4182−4186.

(55) Joly, J.; Khalfallah, M.; Bianchi, D.; Pajonk, G. Acidity of a Microporous Amorphous Alumina Measured by Intermittent Temperature-Programmed Desorption of Ammonia. *Appl. Catal., A* **1993**, *98*, 61−70.

https://doi.org/10.1021/acscentsci.1c00370
ACS Cent. Sci. 2021, 7, 1066−1072